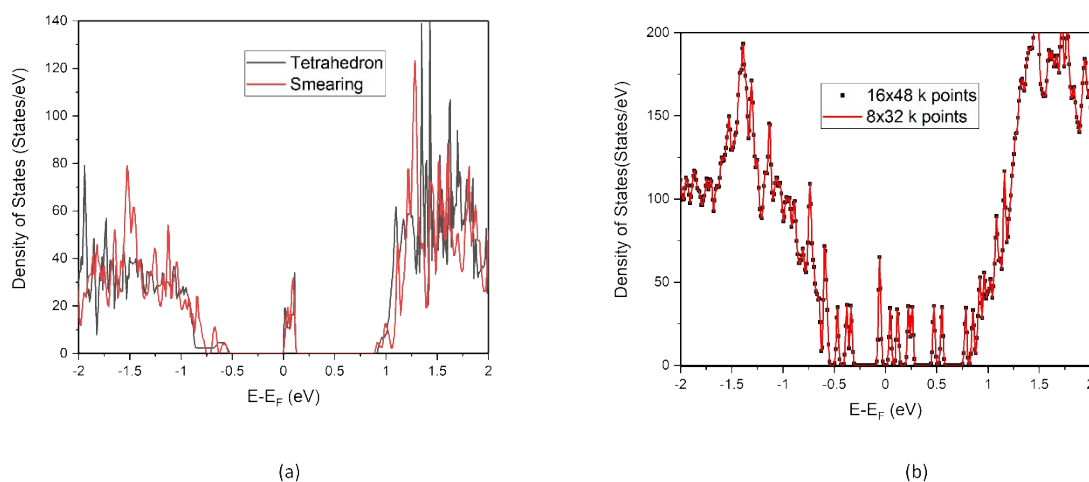


## Supplementary Information

### SI Section 1: Optimisation of K-grid and method of intergration for DOS calculation

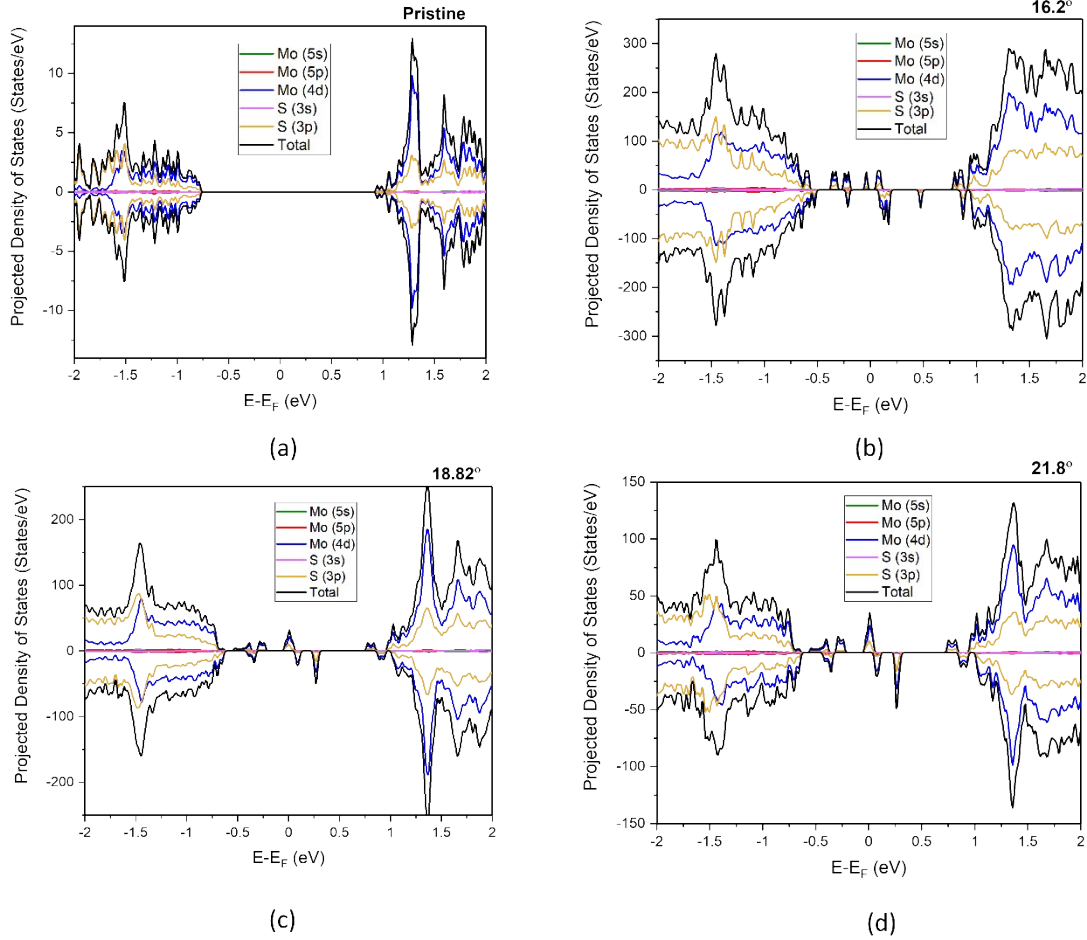
To confirm that the method of integration does not significantly effect the grain boundary DOS, we have performed DOS calculation on quantum espresso using tetrahedron method of integration on 60° grain boundary as shown below in SI Figure 1(a). It can be observed that the DOS from both the calculations are nearly same features at the fermi level and for VBM and CBM. To further confirm the independence of the DOS on k points we have calculated DOS on 16 x 48 kpoints and we observe that the result is consistent with 8 x 32 kpoints



SI Figure.1. (a) DOS calculation from different methods of intergration of Briollouin zone (b) DOS calculation on different k grids.

### SI Section 2: Spin-polarised calculation on grain boundaries

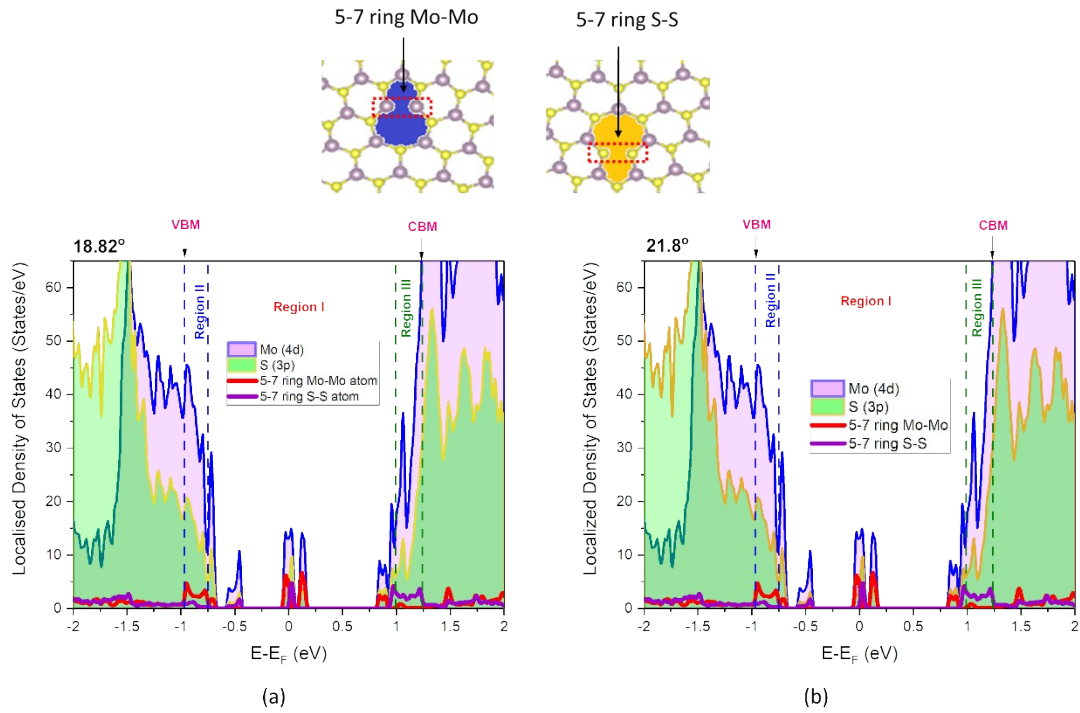
We conducted spin polarised calculations for a few grain boundaries and also observed non-spin degenerate states in the mid-gap region which are localized to the defect states. They arise predominantly from the Mo  $4d_{x^2-y^2,xy}$  and  $4d_{z^2}$  along with a some contributions from the S  $3P_x$  states. The spin non-degeneracy energy differences fall well below the thermal energy scales considered here and showed only minor magnetism of 0.1-0.2  $\mu\text{B}/\text{nm}$  were observed. This small magnetism doesn't affect the transport characteristics and hence we have considered spin polarisation for other calculations.



SI Figure.2. Spin polarised DOS calculations of (a) Pristine and various grain boundaries such as (b)  $16.2^\circ$  (c)  $18.82^\circ$  (d)  $21.8^\circ$ .

### Section 3: LDOS of $18.82^\circ$ and $21.8^\circ$ mirror-oriented grain boundary structure

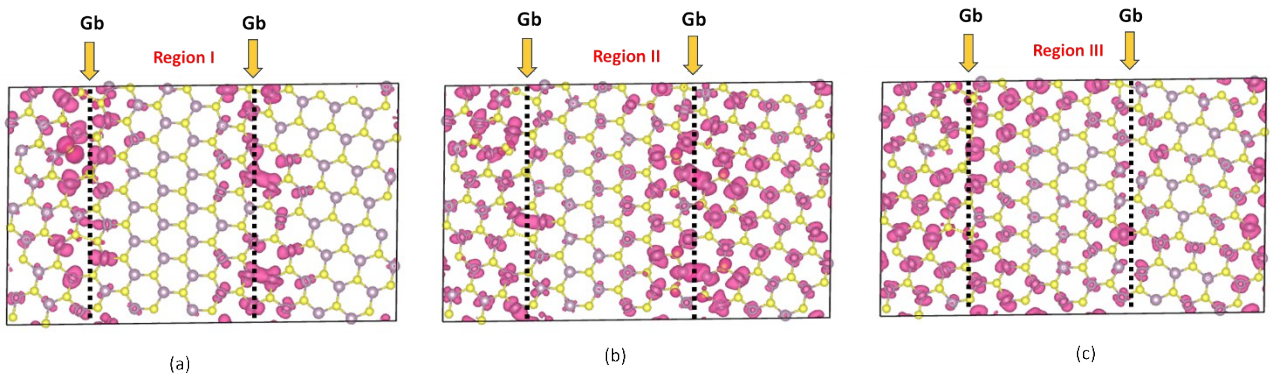
The individual defect atoms and its contribution to the states for  $18.82^\circ$  and  $21.8^\circ$  is presented in SI Figure.3. It can be observed that the Mo and S homoelemental bonds belonging to the 5-7 rings present its states both at the fermi level and in the continuous states region. More specifically, the Mo atoms of homoelemental bond present states at the continuous states region near VBM while S atoms of homoelemental bond present states at the continuous states region above CBM.



SI Figure.3. (a) Localised Density of States of (a)  $18.82^\circ$  and (b)  $21.8^\circ$  misoriented grain boundary structure

Section 4: LDOS isosurface plot of  $21.8^\circ$  misoriented asymmetric grain boundary structure.

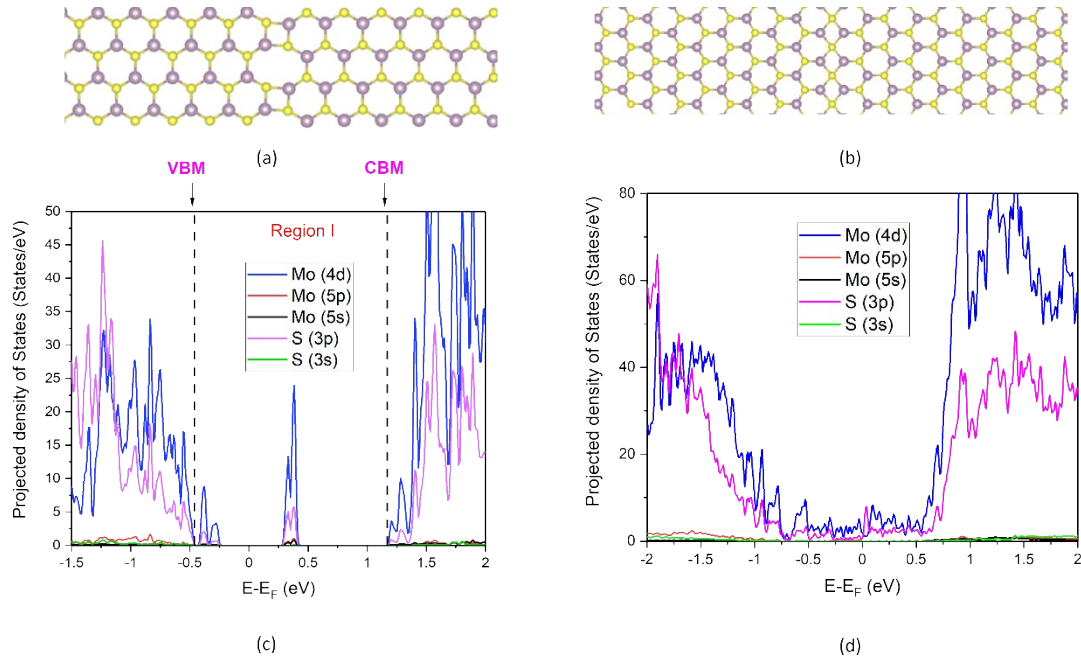
The isosurface plot of  $21.8^\circ$  misoriented asymmetric grain boundary structure corresponding to various regions are shown in SI Figure.4. Region 1 shows the mid gap states contribution of various atoms, it can be seen that the Region 1 is highly localised to the defects states. While Region II and Region III are comparatively weakly localised to Region I, Thus Region I act as deep trap, while Region II and Region III act as shallow traps.



SI Figure.4. Localised Density of States isosurface plot of  $21.8^\circ$  misoriented grain boundary structure corresponding to (a) Region 1 (b) Region II and (c) Region III as marked in Figure 5(b) of main text.

Section 5: 4-8 rings and 4-4 rings Grain boundary's structure

$60^\circ$  grain boundary depending on the edge configuration (armchair or zig-zag) shows wide range of defect structures. SI Figure.5. shows  $60^\circ$  grain boundary having (a) 4-8 defects ring and (b) 4-4 defect rings and corresponding density of states shown in SI Figure.5 (c) and (d) respectively. The 4-8 membered ring defect structure, presents states only in the forbidden region and thus this structure has same bandgap as the pristine. While the 4-4 membered ring grain boundary presents states at all the energy level and therefore is metallic in nature.



SI Figure.5. Grain boundary structure of  $60^\circ$  misoriented boundary having (a) 4-8 defect structure and its corresponding PDOS (b) 4-4 defect structure and its corresponding PDOS.